ACS OMEGA

http://pubs.acs.org/journal/acsodf

Article

Arene–Ruthenium(II) Complexes Containing 11*H*-Indeno[1,2-*b*]quinoxalin-11-one Derivatives and Tryptanthrin-6-oxime: Synthesis, Characterization, Cytotoxicity, and Catalytic Transfer Hydrogenation of Aryl Ketones

Vladislava V. Matveevskaya, Dmitry I. Pavlov, Taisiya S. Sukhikh, Artem L. Gushchin, Alexander Yu. Ivanov, Tatiana B. Tennikova, Vladimir V. Sharoyko, Sergey V. Baykov, Enrico Benassi,* and Andrei S. Potapov*

Cite This: https://dx.doi.org/10.1021/acsomega.0c01204

Read Online

ACCESS | Metrics & More | Article Recommendations | Supporting Information

ABSTRACT: A series of novel mono- and binuclear arene–ruthenium(II) complexes [(*p*-cym)Ru(L)Cl] containing 11*H*-indeno[1,2-*b*]quinoxalin-11-one derivatives or tryptanthrin-6-oxime were synthesized and characterized by X-ray crystallography, IR, NMR spectroscopy, cyclic voltammetry, and elemental analysis. Theoretical calculations invoking singlet state geometry optimization, solvation effects, and noncovalent interactions were done using density functional theory (DFT). DFT calculations were also applied to evaluate the electronic properties, and time-dependent DFT was applied to clarify experimental UV–vis results. Cytotoxicity for cancerous and noncancerous human cell lines was evaluated with cell viability MTT assay. Complexes demonstrated a moderate cytotoxic effect toward cancerous human cell line PANC-1. The catalytic activity of the complexes was evaluated in transfer hydrogenation of aryl ketones. All complexes exhibited good catalytic activity and functional group tolerance.

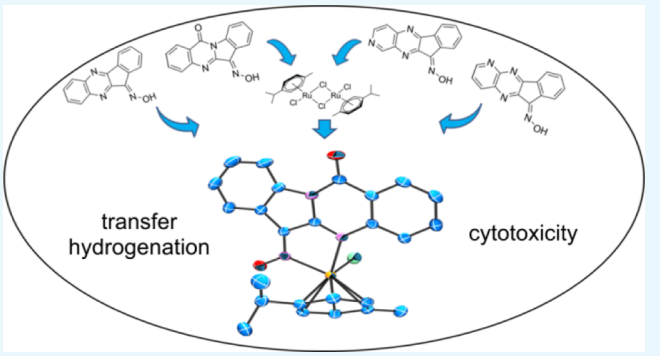

INTRODUCTION

Chemistry of half-sandwich arene–ruthenium(II) complexes has been intensively investigated in the recent years, due to their applications in different areas such as catalysis and pharmacology. Such complexes demonstrated high antiviral,[1−3] antibiotic,[3−6] and antitumor[7−17] activity.

Ruthenium(II) coordination compounds also have been extensively investigated for their catalytic activity in transfer hydrogenation reactions[18−27] and metathesis polymerization.[28−30]

Arene–ruthenium complexes have piano-stool type geometry with pseudo-octahedral symmetry near the ruthenium(II) atom. The arene fragment stabilizes the complex and protects the Ru(II) metal center from oxidation to ruthenium(III). Aromatic ligands are relatively inert in substitution reactions and can be considered as spectator ligands. The three remaining coordination sites opposite to the arene ligand can be used to introduce a wide variety of ligands with N-, O-, S- or P-donor atoms. In the past decade, there has been a surge of interest in nitrogen-donor ligands for use in catalysis and bidentate ligands have been very successful in this area.

Our group is involved in the research of polycyclic N-containing ligands—oximes of 11*H*-indeno[1,2-*b*]quinoxalin-11-one and its structural analogues.[31] 11*H*-Indeno[1,2-*b*]quinoxalin-11-one oxime, often denoted in the literature as IQ1, and its sodium salt, IQ1S, were reported as potent c-Jun N-terminal kinase (JNK3) inhibitors,[31,32] anti-inflammatory agents,[33−35] neuroprotectors,[36,37] and antitumor agents.[38−40] Tryptanthrin demonstrates a wide range of bioactivities,[41,42] including antibacterial,[43,44] antiviral,[45] anticancer,[46,47] and anti-inflammatory[48] activity. However, the coordination chemistry of such compounds is insufficiently explored. There are only few examples of nickel(II) and cobalt(II) complexes with 11*H*-indeno[1,2-*b*]quinoxalin-11-one oxime, which to the best of our knowledge has never been employed before in the synthesis of any noble metal complexes. Such oxime ligands as 11*H*-indeno[1,2-*b*]-quinoxalin-11-one oxime in the presence of base (NEt_3) can

Received: March 18, 2020
Accepted: April 28, 2020

adopt up to eight different coordination modes, leading to Ni(II) and Co(II) complexes with nuclearities ranging from 1 to 8.[49,50] 11*H*-Indeno[1,2-*b*]quinoxalin-11-one oxime and its derivatives look promising in terms of stabilizing the complexes due to $\pi-\pi$ stacking interactions and its coordinating ability. Herein, we report the first examples of arene−Ru(II) complexes with 11*H*-indeno[1,2-*b*]quinoxalin-11-one oximes and tryptanthrin-6-oxime, a derivative of natural alkaloid tryptanthrin. It was shown that such polycyclic oximes are capable of acting as chelating ligands, forming mono- and binuclear coordination compounds.

RESULTS AND DISCUSSION

Synthesis of the Complexes. The ligands used in this work and their abbreviations are summarized in Scheme 1.

Scheme 1. Structures of Ligands HL_1−HL_4

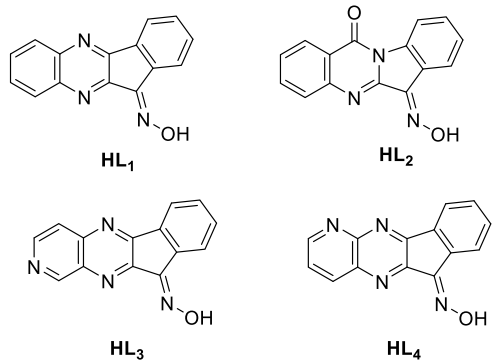

Complexes **1**, **2**, and **4** were prepared in high yield by the reaction between the commercially available arene−ruthenium dimer $[Ru(p\text{-cym})Cl_2]_2$ and the appropriate ligand in methanol/dimethylformamide (DMF) mixture (complexes **1**, **4**) or methanol (complexes **2**, **3**). It was shown that even in the absence of a base, deprotonation of the oxime group occurs, and the ligands (HL_1, HL_2, and HL_4) are coordinated in anionic form. It is worth noting that complex **3** could be obtained only in the presence of a base. Complex **3** was prepared by the reaction between $[Ru(p\text{-cym})Cl_2]_2$ and HL_3 in methanol in the presence of KOH. Ligands HL_1 and HL_2 form mononuclear complexes of the typical piano-stool type (Scheme 2).

Ligands HL_3 and HL_4 contain an additional nitrogen atom; therefore, they can form both mono- and binuclear complexes.

Scheme 2. Synthesis of Complexes 1−2

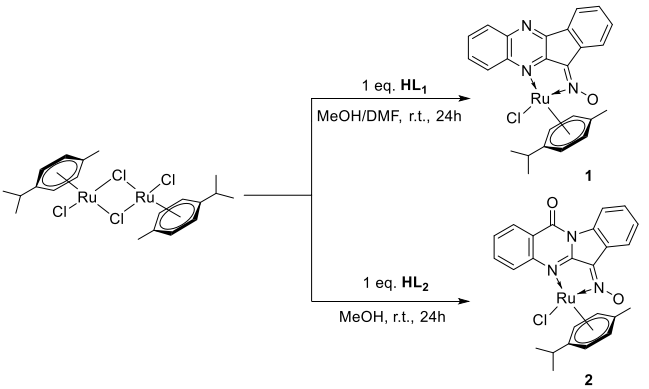

Unexpectedly, the ratio of the reagents did not affect the product composition: at a ratio of Ru/HL_3 2:1, ligand HL_3 forms a binuclear complex **3** of composition $[Ru_2(p\text{-cym})_2(L_3)Cl_3]$, whereas at a ratio of 1:1 instead of a mononuclear complex, the product contains the same complex **3** and the initial ligand (Scheme 3).

Scheme 3. Synthesis of Complex 3

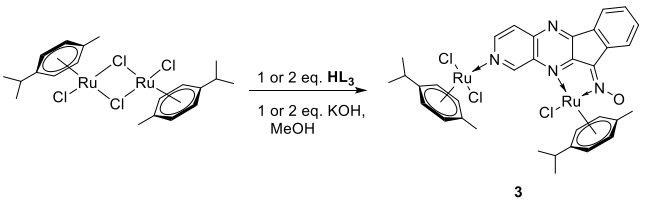

Similarly, reaction between HL_4 and $[Ru(p\text{-cym})Cl_2]_2$ is not affected by reactants ratios. Regardless of the metal−ligand ratio, only mononuclear complex of the composition $[Ru(p\text{-cym})(L_4)Cl]$ was obtained (Scheme 4). In this case,

Scheme 4. Synthesis of Complex 4

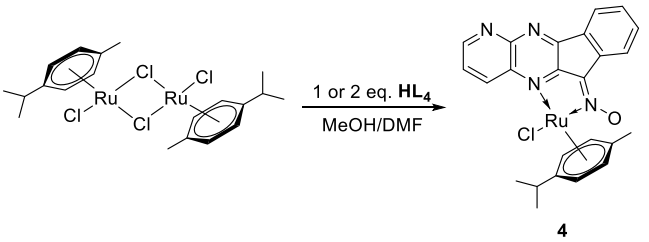

the formation of a dinuclear complex (*via* nitrogen donor atom in position 1 of the tetracyclic system) is probably hindered by the repulsion between the lone pair of the nitrogen atom in position 11 and bulky Ru(cym) fragment.

All complexes are air-stable in the solid state; they are sparingly soluble in chloroform, acetonitrile, and DMSO and almost insoluble in water and alcohols. The complexes were fully characterized by elemental analysis, cyclic voltammetry, IR, NMR spectroscopy methods, and single-crystal X-ray diffraction.

Coordination of anionic forms of the ligands HL_1−HL_4 with strong electron-withdrawing indeno[1,2-*b*]quinoxaline or tryptanthrin cores may be due to increased acidity of these ligands compared to the oximes of aliphatic or aromatic ketones, leading to increased concentration of their anionic forms. Thermochemical density functional theory (DFT) calculations were carried out in order to compare the thermodynamic stability of the complex 1 and its hypothetical form with the neutral coordinated HL_1 ligand. Two reactions of formation of both of the complexes were considered

$$L_1^- + [Ru(cym)Cl_3]^- = [Ru(cym)(\mathbf{L})Cl] + 2Cl^- \quad (1)$$

$$HL_1 + [Ru(cym)Cl_3]^- = [Ru(cym)(\mathbf{HL_1})Cl]^+ + 2Cl^- \quad (2)$$

Free-energy and enthalpy changes were calculated at M062X 6-311+G(2d,p)/LANL2DZ level of theory, and solvent (DMF) effects were taken into account using SMD model. It was found that the formation of the complex with the anionic form is more thermodynamically favorable (ΔG_1 =

https://dx.doi.org/10.1021/acsomega.0c01204
ACS Omega XXXX, XXX, XXX−XXX

−94.9 kJ/mol; ΔG_2 = −16.3 kJ/mol; ΔH_1 = −97.6 kJ/mol; ΔH_2 = −10.8 kJ/mol).

X-ray Crystal Structures. Complexes **1**−**4** crystallize in a monoclinic crystal system having a single formula unit as an asymmetric unit. Phase purity of the obtained products was confirmed by powder X-ray diffraction analysis (see the Supporting Information). In mononuclear complexes **1**, **2**, and **4**, ruthenium coordinates cymene molecule in a η^6 fashion, which is considered to occupy three coordination sites of a quasi-octahedral arrangement. The other three sites are occupied by a chlorine atom and two nitrogen atoms of the deprotonated oximate ligands coordinated in a bidentate fashion forming a five-membered chelate ring (Figures 1−3).

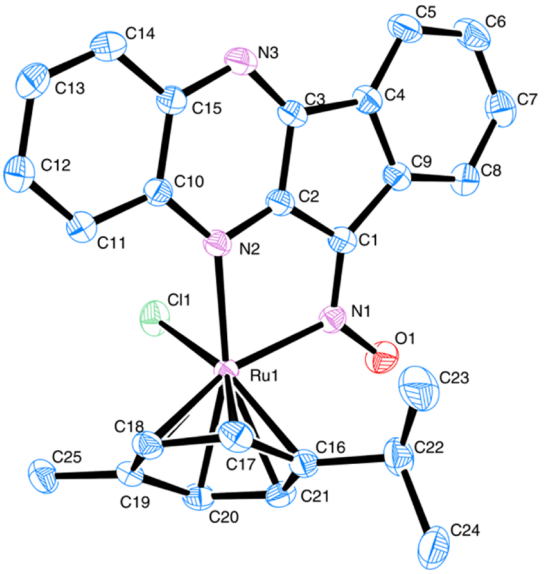

Figure 1. X-ray molecular structure of complex **1**. Thermal ellipsoids are drawn at a 50% probability level. Hydrogen atoms are omitted for clarity. Selected bond lengths [Å]: Ru1−N1 2.101(1), Ru1−N2 2.147(1), Ru1−Cl1 2.4066(5), Ru1−C16 2.193(2), Ru1−C17 2.175(2), Ru1−C18 2.256(2), Ru1−C19 2.264(2), Ru1−C20 2.186(2), Ru1−C21 2.181(2).

It should be noted that in most of the structurally characterized arene−ruthenium complexes with heterocyclic oximes, the N,N-coordinated ligands remain neutral[51−54] and so far only one example of deprotonated 2-pyridyl cyanoxime was reported.[51]

The interatomic Ru−N distances involving oxime and heterocyclic nitrogen atoms are in the ranges of 2.08−2.10 and 2.12−2.16 Å and somewhat greater than the corresponding values typical for oxime−ruthenium complexes (1.95−2.04 and 1.95−2.08 Å), probably due to bulkiness of the ligands. The interatomic Ru−Cl distances of about 2.40 Å and Ru−C distances in the range 2.17−2.26 Å are close to typically found in arene−ruthenium complexes. All three complexes have chiral metal centers, but crystallize in a centrosymmetric space group, and thus, enantiomer resolution was not possible.

Compound **3** is a binuclear complex that crystallizes in a centrosymmetric monoclinic *C*2/*c* space group (Figure 4). Arrangement of one of ruthenium atoms is similar to mononuclear complexes described above—it consists of two nitrogen atoms of deprotonated oxime ligand $\mathbf{HL_3}$, chloride ion and *p*-cymene molecule, interatomic distances between ruthenium and donor atoms are also close to the ones

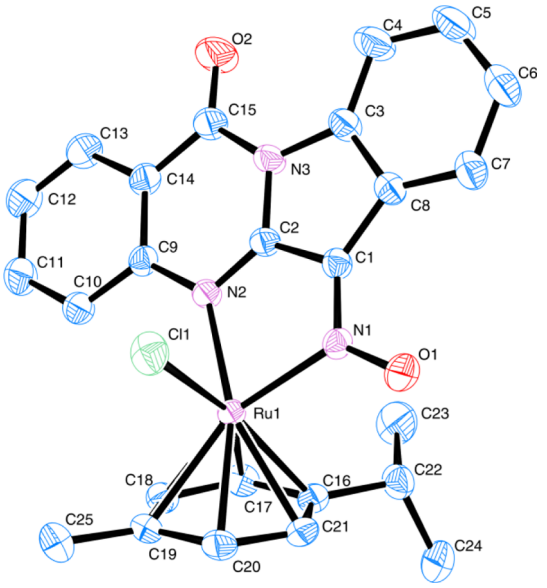

Figure 2. X-ray molecular structure of complex **2**. Thermal ellipsoids are drawn at a 50% probability level. Hydrogen atoms are omitted for clarity. Selected bond lengths [Å]: Ru1−N1 2.079(1), Ru1−N2 2.159(1), Ru1−Cl1 2.4041(7), Ru1−C16 2.200(1), Ru1−C17 2.177(2), Ru1−C18 2.255(1), Ru1−C19 2.265(2), Ru1−C20 2.183(2), Ru1−C21 2.180(2).

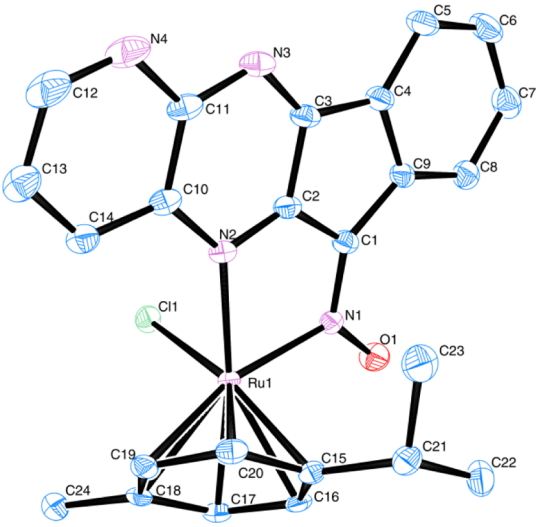

Figure 3. X-ray molecular structure of complex **4**. Thermal ellipsoids are drawn at a 50% probability level. Hydrogen atoms and DMF solvent molecules are omitted for clarity. Selected bond lengths [Å]: Ru1−N1 2.094(2), Ru1−N2 2.124(2), Ru1−Cl1 2.4031(6), Ru1−C15 2.212(2), Ru1−C16 2.172(2), Ru1−C17 2.189(2), Ru1−C18 2.260(2), Ru1−C19 2.249(2), Ru1−C20 2.171(2).

observed for mononuclear complexes. The second ruthenium atom is achiral and coordinates one cymene molecule, two chloride ions, and a nitrogen atom in position 2 of ligand $\mathbf{HL_3}$.

In complexes **1** and **2** the heterocyclic oxime ligands are involved in $\pi-\pi$ stacking with intermolecular distances 3.379(3) and 3.384(2) Å correspondingly (Figures S1 and S2). In compound **4**, the molecules of ligand $\mathbf{HL_4}$ cannot align in parallel planes due to the presence of lattice DMF molecules. In this case, each of $\mathbf{HL_4}$ molecules is involved in four CH···N short contacts with interatomic H···N distances of 2.658 and 2.741 Å (Figure S3).

https://dx.doi.org/10.1021/acsomega.0c01204
ACS Omega XXXX, XXX, XXX−XXX

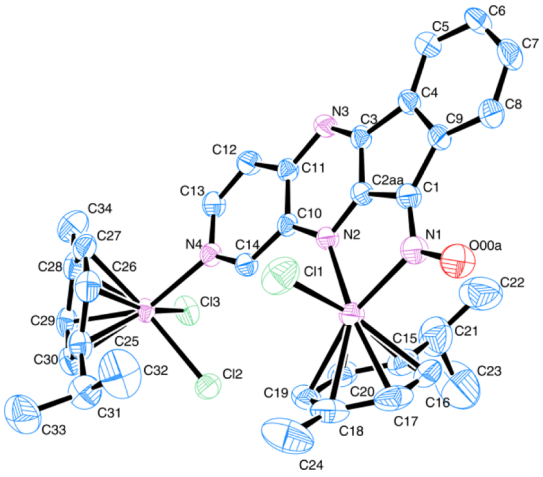

Figure 4. X-ray molecular structure of **3**. Thermal ellipsoids are drawn at a 50% probability level. Hydrogen atoms and MeOH solvent molecules are omitted for clarity. Selected bond lengths [Å]: Ru1−N1 2.096(2), Ru1−N2 2.124(2), Ru1−Cl1 2.387(2), Ru1−C15 2.207(5), Ru1−C16 2.146(6), Ru1−C17 2.182(4), Ru1−C18 2.238(3), Ru1−C19 2.230(3), Ru1−C20 2.189(4), Ru1−N4 2.134(2), Ru1−Cl2 2.425(1), Ru1−Cl3 2.412(1), Ru1−C25 2.203(4), Ru1−C26 2.179(5), Ru1−C27 2.153(5), Ru1−C28 2.187(5), Ru1−C29 2.169(4), Ru1−C30 2.183(3).

In order to provide a quantum mechanical foundation to the experimental observations, the analysis of the non-covalent interaction (NCI) isosurfaces was performed both on monomers and dimers of compounds **1**, **2**, and **4** (Figure S4). The intramolecular interactions that are mainly responsible for the stabilization of the monomers (blue areas) involve hydrogen atoms, which are involved in attractive interactions with the two oxygen atoms, carbon atoms, and with the chlorine atom. Concerning dimers, the main contribution to the stabilization of $\mathbf{1}_2$ and $\mathbf{2}_2$ is a wide $\pi-\pi$ interaction between two ligands; the case of $\mathbf{4}_2$ is rather different, by involving four punctual but more attractive interactions between hydrogen atoms of one ligand and nitrogen atoms of the other ligand molecule (Figure S4).

Thermodynamic preference of *N,N*-bidentate over *N,O*-bidentate coordination mode of the ligand $\mathbf{L_1}$ was confirmed by DFT calculations. Both in the gas phase and DMF N,N-coordination of the deprotonated ligand $\mathbf{L_1}$ with the formation of a five-membered ring is about 19 kJ/mol more favorable (Figure S5).

Two possible orientations of the cymene ligand—one with isopropyl group close to the oxime fragment and the other with the opposite orientation—methyl group facing the oxime were evaluated by DFT calculations (Figure S6). It was found that the first orientation is about 8 kJ/mol more stable than the second one consistent with the X-ray crystal structures. Despite the proximity of the bulky isopropyl group and the oxime fragment, this form is more stable probably due to the repulsion of the isopropyl group and the aromatic part of the HL1 ligand in the structure with the opposite cymene orientation.

Spectroscopic Characterization. The IR spectra of free neutral ligands display broad bands in the range 3200−3250 cm^{-1} due to OH stretching vibrations and bands in the range 1640−1630 cm^{-1} due to C═N stretching vibrations. Upon coordination OH stretching bands disappear, whereas C═N stretching bands shift to 1625−1600 cm^{-1}, in accordance with the deprotonation of the ligands and their coordination to the metal center in *N,N′*-bidentate chelating fashion.

The ^{1}H NMR spectra of complexes **1**−**4** recorded in DMSO-d_6 display all of the expected signals of the coordinated *p*-cymene and N,N′-ligand. The resonances of the N,N′-ligand atoms are shifted upfield with respect to those of uncoordinated ligands, confirming its coordination to the ruthenium(II) center. The chirality of ruthenium center in the complexes induces significant changes to the NMR signals of the *p*-cymene moiety in complexes **1**−**4**. The ^{1}H NMR spectra of **1**, **2**, and **4** exhibit a doublet of doublets for the methyl groups in the isopropyl moiety, and four doublets attributable to the protons of *p*-cymene ring in the range of 5.5−6.3 ppm, which is typical of ruthenium−arene systems with an asymmetric ruthenium center.[55,56] The ^{1}H NMR spectra of binuclear complex **3** exhibit two doublets of doublets for the methyl groups in the isopropyl moiety, and eight doublets attributable to the *p*-cymene protons in the range of 5.3−6.2 ppm. There is no signal of the oxime proton in the spectra of all complexes, which confirms the coordination of the ligand in the anionic form. All complexes demonstrate resonances in the range typical of related compounds and in accordance with the existence of only one species in solution.

UV−vis spectrum of complex **1** (Figure S7) in acetonitrile demonstrates a complex shape that can be deconvoluted into five Gaussian bands (Figure S8). In order to gain insight into the origin of the absorption bands, time-dependent DFT calculations were carried out (Figure S9). The main features of the singlet excited states showing the highest values of oscillator strength (*f*) together with the experimental positions of deconvoluted Gaussian bands are given in Table 1. Because of the complexity of the transition nature in terms of MOs elementary transitions, the natural transition orbital (NTO) analysis was also carried out. As it can be seen from the transition diagrams, all of the absorption bands are of mixed character and correspond to both local and charge transfer excitations. Although the nature of the longer absorption transitions (500−260 nm) is charge transfer, calculations performed by employing long-range corrected hybrid functionals (*viz.* CAM-B3LYP and *ω*-B97X[D]) did not show a significant improvement in the match with the experimental values with respect to the B3LYP functional; on the contrary, for the short wavelength region transitions (200−230 nm), *ω*-B97X[D] demonstrated a good performance.

Cyclic Voltammetry Studies. To study the redox properties of mononuclear and binuclear complexes **1** and **3** in solution, cyclic voltammograms were recorded at room temperature and a scan rate of 0.1 V/s using a 0.1 M solution of Bu_4NPF_6 in DMF (Figures S10 and S11). The corresponding values $E_{1/2}$ of the redox potentials are shown in Table 2. In the positive region, an anodic peak was detected at +1.30 and +1.37 V (versus Ag/AgCl) for complexes **1** and **3**, respectively. These irreversible processes apparently correspond to the oxidation of Ru(II) to Ru(III). This is consistent with the fact that the highest occupied molecular orbital in **1** is partially localized on the ruthenium atom (8,5%, Table S1). Sufficiently high oxidation potentials are consistent with the *π*-acceptor properties of heterocyclic oxime and *p*-cymene ligands. Ru-centered oxidation in the region from +1.0 to +1.5 V (vs Ag/AgCl) was also found for similar *p*-cymene complexes of Ru(II).[57,58] The irreversibility of this process is probably due to the instability of the *p*-cymene−

https://dx.doi.org/10.1021/acsomega.0c01204
ACS Omega XXXX, XXX, XXX−XXX

Table 1. TDA−DFT (B3LYP 6-311+G(2d,p)/LANLDZ IEFPCM) Calculated Singlet Excited States and Experimental Absorption Maxima in the UV−Vis Spectrum of Complex 1

Excited state	Oscillator strength	λ_{calc}, nm	λ_{exp}, nm	NTO transitions	NTO diagrams
S1	0.0029	506	515	117 → 118 (0.96)	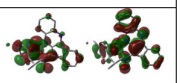
S4	0.0227	432	450 sh.	117 → 118 (0.79) 116 → 119 (0.15)	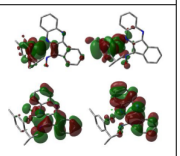
S11	0.1010	360	368	117 → 118 (0.46) 116 → 119 (0.39) 115 → 120 (0.13)	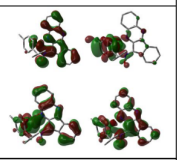
					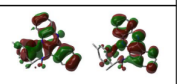
S16	0.1376	331	333	117 → 118 (0.58) 116 → 119 (0.20) 115 → 120 (0.13)	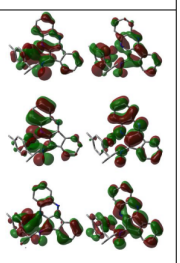
S38	0.5556	257	267	117 → 118 (0.42) 116 → 119 (0.26)	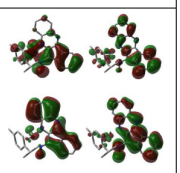
S35[a]	0.201	227	230	117 → 118 (0.36) 116 → 119 (0.21) 115 → 120 (0.16) 114 → 121 (0.11)	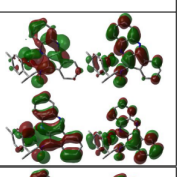
					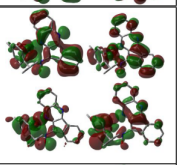
S50[a]	0.0928	200	201	117 → 118 (0.37) 116 → 119 (0.26) 115 → 120 (0.16)	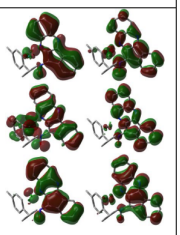

[a]Values calculated using ω-B97X[D] 6-311+G(2d,p)/LANLDZ IEFPCM method.

Ru(III) species and the removing of the *p*-cymene fragment. This is evidenced by the elongation of Ru−C bonds and a loss in energy during the transition from Ru(II) complex to Ru(III) complex according to DFT calculations.

Table 2. Redox Potentials[a] (V, vs Ag/AgCl) for Complexes 1, 3, and HL_1

compound	E_p^{ox}	E_p^{red}
1	+1.30	−1.06, −2.06
3	+1.37	−0.85, −1.82
HL_1[b]		−1.80, −2.21

[a]Determined in 0.1 M Bu_4NPF_6 in DMF at room temperature and a scan rate of 0.1 V/s. [b]In CH_3CN.

A number of irreversible processes were detected in the negative region both for complexes **1** and **3**, probably related to the reduction of the heterocyclic oxime ligand. This is consistent with the composition of lowest unoccupied molecular orbital in **1**, which mainly consists of the oxime ligand orbitals (53%, Table S1). Similar irreversible reduction processes shifted to a more cathodic region were also found in the cyclic voltammogram of the starting HL_1 ligand in acetonitrile (Figure S12).

Catalytic Activity Studies. We have tested the catalytic activity of complexes for the selective hydrogenation of aryl ketones using 2-propanol as both the reducing agent and solvent in the presence of NaOH as the base. Reaction between isopropyl alcohol and acetophenone was chosen as a model reaction (Scheme 5).

Scheme 5. Ru-Catalyzed Transfer Hydrogenation of Aryl Ketones

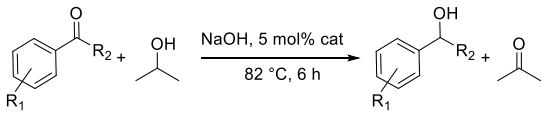

Reduction of acetophenone did not go to completion (Table 3), which can be explained by the reversibility of hydrogen transfer. Conversion versus time plots for complexes **1**−**4** are shown in Figure 5. Complex **1** demonstrated the best catalytic activity, providing 93% conversion after 1 h. Other complexes (**2**−**4**) gave ∼50% conversions after 1−2 h, and nearly full conversion for catalysts **2** and **3** was achieved in 6 h.

Table 3. Transfer Hydrogenation of Acetophenone Catalyzed by Complexes 1—4

bomplex	yield, %[a]	TON	TOF, h^{-1}
1	93	18	18
2	95	19	5
3	93	18	6
4	69	13	2

[a]Reactions were carried out in 2-propanol(4.0 mL), in the presence of NaOH (0.1 mmol), acetophenone (1 mmol), and catalyst (0.05 mmol) at 82 °C during 6 h [Ru]/substrate/NaOH molar ratio = 1/20/2. Hydrogenated products were determined by gas chromatography using phenetole as internal standard. TON = *turnover number* = mol of product/mol of pre-catalyst. TOF = *turnover frequency* = mol of product/mol of pre-catalyst/time.

Encouraged by the potential of complex **1**, we were interested to test this complex for transfer hydrogenation of substituted aryl ketones (Scheme 5), and complex **1** was

https://dx.doi.org/10.1021/acsomega.0c01204
ACS Omega XXXX, XXX, XXX−XXX

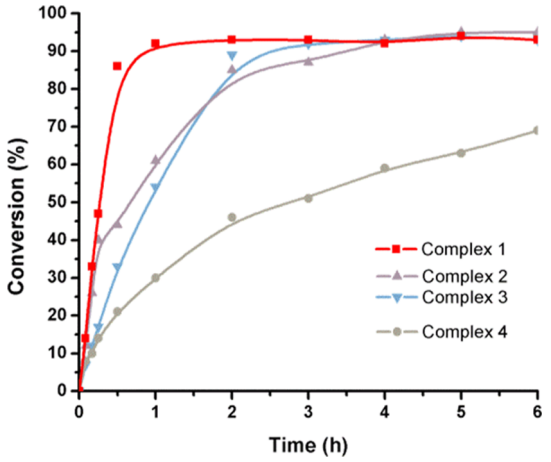

Figure 5. Conversion versus reaction time for acetophenone transfer hydrogenation.

found to exhibit good catalytic activity and functional groups tolerance (Table 4).

Conversion versus time plots for the five ketones (Table 4, entries 2−6) are shown in Figure 6. It was shown that ketones with electron-donating groups reacted faster. It might be due to the increase of the electron density on the carbon atom of the carbonyl group, which favorably affects the coordination of the carbonyl group to ruthenium(II) center. In turn, electron-withdrawing substituents (Table 4, entries 6, 7) reduce the electron density on the carbonyl group of the substrate, which makes coordination to the ruthenium(II) more difficult, which results in the decrease of the reaction rate.

High chemoselectivity of the reduction process was noted: nitro groups (Table 4, entries 6, 7) remain unchanged under the hydrogenation conditions. For ketone with the double C═C bond conjugated to the carbonyl group (Table 4, entry 8), only ketone moiety undergoes transformation. Moreover, high yields can also be achieved in case of 4-bromooacetophenone hydrogenation (Table 4, entry 5), with no evidence of dehydrobromination or ring reduction. It is worth noting that a heteroaromatic ketone can also be reduced (Table 4, entry 10). Pyridine moiety can potentially bind to ruthenium center and inhibit the catalytic reaction; however, 2-acetylpyridine (Table 4, entry 10) was rapidly hydrogenated.

Cytotoxicity. Pancreatic cancer is one of the most aggressive and deadly types of cancer. The increasing resistance of the pancreatic cancer to effective chemotherapy has become an urgent problem.[59] Therefore, the obtained complexes were screened at different concentrations for their ability to affect the cell viability of human adenocarcinoma cell line PANC-1 over noncancerous human retinal pigment epithelial cell line ARPE-19. The cytotoxic activity of the complexes was analyzed by cell viability MTT assay.

As it is shown in Figure 7, complexes **1**−**3** demonstrate moderate cytotoxic effect toward PANC-1 but practically no cytotoxic effect ARPE-19 cell lines. Complex **2** at the concentrations of 30 and 90 μM decreased cell viability for PANC-1 cell line to 95 and 70%, respectively. Complex **4** at the concentrations 0.3, 30, and 90 μM decreased cell viability for PANC-1 cell line to 55, 40, and 55%, respectively. It can be concluded that complexes **2** and **4** have mild cytotoxic activity for cancer human cell lines. Nevertheless, the cytotoxicity of the studied complexes is significantly inferior to the cytotoxicity of drugs widely used in clinical practice for the chemotherapeutical treatment of pancreatic adeonocarcinoma, that is, fluorouracil (IC_{50} 3.85 μM) and gemcitabine

Table 4. Transfer Hydrogenation of Aryl Ketones Catalyzed by Complex 1

Entry	Substrate	Product	Yield, % [a]
1			93
2	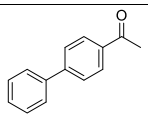	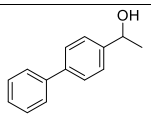	80
3	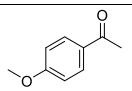	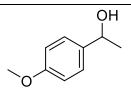	82
4	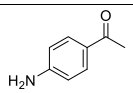	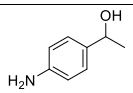	76
5	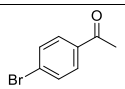	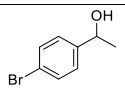	71
6	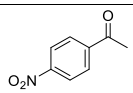	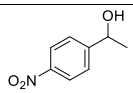	59
7	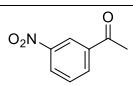	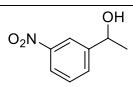	57
8	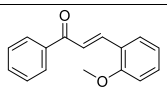	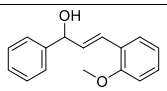	81
9	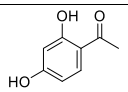	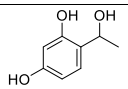	79
10			82

[a]Hydrogenated products were determined by gas chromatography using phenetole as internal standard.

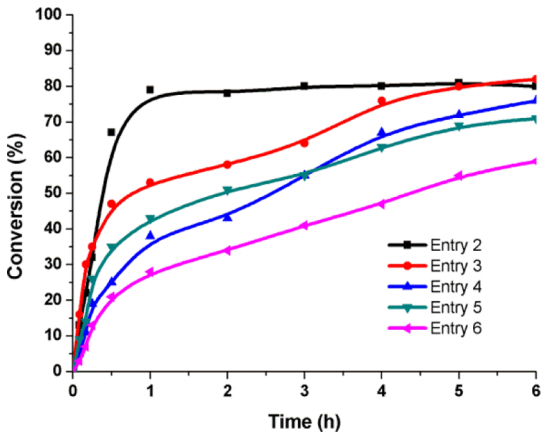

Figure 6. Conversion versus time plots (entries 2−6 in Table 4).

https://dx.doi.org/10.1021/acsomega.0c01204
ACS Omega XXXX, XXX, XXX−XXX

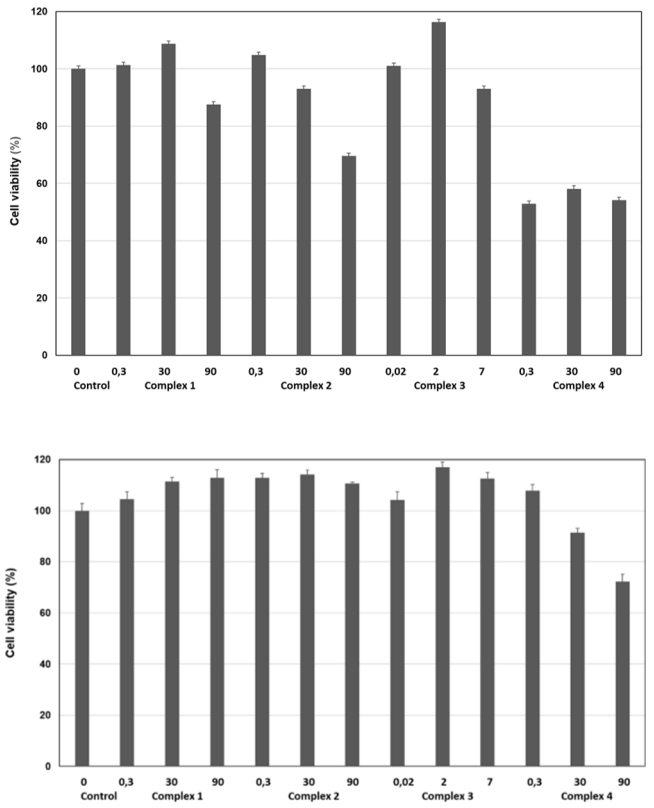

Figure 7. Cell viability MTT assay results for complexes **1**−**4** against PANC-1 (top) and ARPE-19 (bottom) cell lines (values are shown as the mean ± SEM of four experiments, the concentrations of the complexes on the horizontal axis are given in μM).

(IC_{50} 27 nM).[60] It is interesting to note that at low concentrations of the complexes viability of the cells increased (relative to control) despite the known cytotoxic potential of arene−ruthenium core. This is probably due to the JKN3-inhibitive activity of the oxime ligands discovered recently,[31] which limit the cell apoptosis process.

CONCLUSIONS

Ruthenium(II)−arene complexes containing 11*H*-indeno[1,2-*b*]quinoxalin-11-one derivatives and tryptanthrin-6-oxime were prepared and their catalytic, biological, and electrochemical properties were evaluated. The crystal structures of all complexes display a typical piano-stool geometry with ligands N,N′-coordinated to the ruthenium in each case.

Our research also shows that arene−ruthenium(II) complexes with 11*H*-indeno[1,2-*b*]quinoxalin-11-one derivatives and tryptanthrin-6-oxime are effective catalysts for the transfer hydrogenation reaction. These complexes tolerate a range of functional groups and catalyze the reaction, giving target alcohols in high yields. Ruthenium complexes with tryptanthrin-6-oxime and 6*H*-indeno[1,2-*b*]pyrido[3,2-*e*]-pyrazin-6-one oxime demonstrated mild cytotoxic activity for human adenocarcinoma cell line PANC-1.

EXPERIMENTAL SECTION

Materials and Methods. The dimer $[Ru(p\text{-cym})Cl_2]_2$ was purchased from Alfa Aesar. The ligands 11*H*-indeno[1,2-*b*]quinoxalin-11-one oxime (**HL_1**), 6-(hydroxyimino)indolo-[2,1-*b*]quinazolin-12(6*H*)-one (tryptanthrin-6-oxime, **HL_2**), 10*H*-indeno[1,2-*b*]pyrido[3,4-*e*]pyrazin-10-one oxime (**HL_3**), and 6*H*-indeno[1,2-*b*]pyrido[3,2-*e*]pyrazin-6-oneoxime (**HL_4**)

Table 5. Crystallographic Data of the Complexes 1−4

compound	**1**	**2**	**3**	**4**
empirical formula	$C_{25}H_{22}ClN_3ORu$	$C_{25}H_{22}ClN_3O_2Ru$	$C_{35.5}H_{41}Cl_3N_4O_{2.5}Ru_2$	$C_{25.5}H_{24.5}ClN_{4.5}O_{1.5}Ru$
formula weight	516.97	532.97	872.23	554.51
temperature/K	200(2)	298(2)	298(2)	150(2)
crystal system	monoclinic	monoclinic	monoclinic	monoclinic
space group	$P2_1/n$	$P2_1/n$	$C2/c$	$P2_1/c$
a/Å	15.3365(10)	15.601(4)	34.0106(13)	18.414(2)
b/Å	8.0892(6)	8.0342(18)	12.5712(5)	16.071(2)
c/Å	17.0781(14)	17.108(4)	20.0181(8)	7.6248(11)
β/deg	93.968(2)	93.210(7)	123.3950(10)	97.453(4)
volume/Å^3	2113.6(3)	2140.9(8)	7145.7(5)	2237.4(5)
Z	4	4	8	4
ρ_{calc}/g/cm^3	1.625	1.654	1.619	1.646
μ/mm^{-1}	0.891	0.886	1.109	0.852
F(000)	1048.0	1080.0	3516.0	1128.0
crystal size/mm^3	0.15 × 0.1 × 0.08	0.3 × 0.25 × 0.25	0.3 × 0.2 × 0.1	0.33 × 0.17 × 0.05
2Θ range for data collection/deg	3.452 to 57.452	3.438 to 57.468	3.544 to 51.466	3.376 to 57.46
index ranges	$-20 \le h \le 13$, $-10 \le k \le 10$, $-23 \le l \le 23$	$-21 \le h \le 21$, $-10 \le k \le 10$, $-23 \le l \le 23$	$-38 \le h \le 41$, $-10 \le k \le 15$, $-24 \le l \le 23$	$-23 \le h \le 24$, $-21 \le k \le 21$, $-7 \le l \le 10$
reflections collected	28,954	31,935	26,579	15,991
independent reflections	5460 [R_{int} = 0.0304, R_{sigma} = 0.0221]	5550 [R_{int} = 0.0243, R_{sigma} = 0.0142]	6810 [R_{int} = 0.0351, R_{sigma} = 0.0354]	5678 [R_{int} = 0.0336, R_{sigma} = 0.0442]
restraints/parameters	0/283	0/292	4/426	12/330
goodness-of-fit on F^2	1.026	1.069	1.020	1.023
final R indexes [$I >\geq 2\sigma$ (I)]	R_1 = 0.0224, wR_2 = 0.0540	R_1 = 0.0190, wR_2 = 0.0508	R_1 = 0.0313, wR_2 = 0.0724	R_1 = 0.0296, wR_2 = 0.0597
final R indexes [all data]	R_1 = 0.0273, wR_2 = 0.0565	R_1 = 0.0211, wR_2 = 0.0525	R_1 = 0.0447, wR_2 = 0.0788	R_1 = 0.0424, wR_2 = 0.0639
largest diff. peak/hole/e Å^{-3}	0.58/−0.34	0.36/−0.43	0.78/−0.40	0.51/−0.78

https://dx.doi.org/10.1021/acsomega.0c01204
ACS Omega XXXX, XXX, XXX−XXX

were prepared as previously described.[36] All other materials were obtained from commercial sources and were used as received.

IR spectra were recorded on an Agilent Cary 630 FTIR spectrometer quipped with a diamond attenuated total reflectance tool from 700 to 3500 cm^{-1}. NMR spectroscopic data were recorded with a Brucker AVANCE III 400 spectrometer (400.13 MHz for ^{1}H and 100.61 MHz for ^{13}C) and were referenced to residual solvent signal.

Chromato-mass spectrometric analysis was carried out using Agilent 7890A gas chromatograph with Agilent 5975C mass-selective detector with quadrupole mass-analyzer (electron impact ionization energy 70 eV). The injector temperature was maintained at 300 °C, and the injection volume was 1 μL (split 40:1). The instrument was equipped with a HP-5 ms capillary column of 30 m length, 0.25 mm i.d., and 0.25 μm film thickness. The carrier gas was helium at a constant flow rate of 1 mL/min. The GC oven program started at 79 °C (1.0 min hold) ramped up to 300 °C (heating rate 13 °C/min) for 10 min, total chromatogram time was 28 min. Transfer line temperature was 300 °C, MS Source—230 °C and MS Quadrouple—150 °C. The electron energy was 70 eV. From 0 to 4 min, the MS was switched off (solvent delay). Data analysis and instrument control was carried out with MSD 5975C software.

Cyclic Voltammetry. Cyclic voltammograms were recorded with a 797 VA Computrace system (Metrohm, Switzerland). All measurements were carried out at room temperature with a conventional three-electrode configuration consisting of glassy carbon working electrode, platinum auxiliary electrode, and Ag/AgCl/KCl reference electrode. The solvent (DMF or CH_3CN) was deoxygenated before use. The solution of tetra-*n*-butylammonium hexafluorophosphate Bu_4NPF_6 (0.1 M) was used as a supporting electrolyte. The concentrations of the compounds were 10^{-3} M.

X-ray Crystallography. Single-crystal X-ray diffraction (XRD) data for the compounds were collected by a Bruker Apex DUO diffractometer using the graphite-monochromated Mo Kα radiation (λ = 0.71073 Å). Absorption corrections were applied with the use of the SADABS program.[61] The crystal structures were solved and refined by means of the SHELXT[62] and SHELXL[63] programs using OLEX2 GUI.[64] Atomic thermal displacement parameters for nonhydrogen atoms except for some solvate molecules were refined anisotropically. The positions of H atoms were calculated corresponding to their geometrical conditions and refined using the riding model. In **3**, O atoms of one of solvate methanol molecules was disordered over three positions with restrained C−O distances (DFIX) and occupancy of 0.33. H atoms of hydroxyl group of methanol molecules were not located but included in the formula of **3**. The crystallographic data and details of the structure refinements are summarized in Table 5. Crystallographic data for the structures **1**−**4** have been deposited with the Cambridge Crystallographic Data Centre (CCDC) as Supporting Information nos. 1974048−1974051. Copies of the data can be obtained free of charge on application to CCDC (http://www.ccdc.cam.ac.uk/data_request/cif).

Catalytic Activity Determination. A typical transfer hydrogenation reaction was carried out under air as follows: to 0.05 mmol of catalyst precursor contained in the reaction flask were added isopropyl alcohol (4 mL), NaOH (0.2 mmol) and acetophenone (1 mmol), in that order. The reaction mixture was stirred for 6 h at 82 °C. After that, reaction mass was analyzed by GC and GC−MS. The performed blank experiments confirmed that no products of reaction were obtained unless the catalyst and NaOH were added.

Cytotoxicity Determination. PANC-1 (pancreatic adenocarcinoma) were obtained from Russian Cell Culture Collection (Institute of Cytology RAS). ARPE-19 (ATCC CRL-2302 retinal pigment epithelial) cells were obtained from the American Type Culture Collection (ATCC) (Manassas, VA). PANC-1 and ARPE-19 cells were cultured in DMEM-F12 medium supplemented with 10% fetal bovine serum, 100 units/mL penicillin, and 100 μg/mL streptomycin, at 37 °C in a humidified atmosphere containing 95% air and 5% CO_2. The cytotoxicity of tested compounds was studied using 3-(4,5-dimethylthiazol-2-yl)-2,5-diphenyltetrazolium bromide (MTT) reduction assay as described previously.[65] MTT-formazan crystals formed by metabolically active cells were dissolved in dimethyl sulfoxide, and absorbance was measured at 540 and 690 nm in Varioskan LUX Multimode Microplate Reader (Thermo Scientific, USA). Values measured at 540 nm were subtracted for background values at 690 nm, and the data were shown as a percent of control untreated samples.

Computational Chemistry Details. The calculations were performed using Gaussian 09 package.[66] Experimental X-ray structures of complex **1** was used as a starting point for DFT geometry optimizations. Singlet state geometry optimizations were carried out at the DFT level of theory employing the three-parameter hybrid B3LYP functional[67−70] and 6-311+G(2d,p) basis set[71−74] for the first and second-row atoms, while LanL2DZ[75,76] was used for the ruthenium atoms. Solvation effects were taken into account using the IEFPCM model[77] and acetonitrile as solvent. Frequency calculations were performed for the optimized geometries in order to establish the nature of the stationary points. Lack of imaginary vibration modes for the optimized structures indicate that the stationary points found corresponded to minima on the potential energy surface. Time-dependent DFT calculations with Tamm−Dancoff approximation[78] were carried out using the same basis sets and B3LYP,[67−70] CAM-B3LYP,[79] and ω-B97X[D][80] functionals. The nature of electronic transitions was analyzed using the NTOs approach.[81] The energies of the coordination isomers of complex **1** were compared after geometry optimization and calculation of vibrational frequencies using M062X[82] functional and 6-311+G(2d,p)/LanL2DZ[75,76] basis sets; solvation effects in dimethylformamide were taken into account using the SMD model.[83]

NCI Analysis by means of the Reduced Density Gradient[84−88] was Performed on the Density of the Optimized Structures Using a Homemade Code. *Synthesis and Characterization. [Ru(p-cym) (L_1)Cl] (**1**).* HL_1 (24.7 mg, 0.1 mmol) was dissolved in DMF (1.5 mL), $[Ru(p\text{-cym})Cl_2]_2$ (30.6 mg, 0.05 mmol) was dissolved in MeOH (1.5 mL), and the resulting solution was added to the initial one. After 24 h, red crystals formed were filtered off and washed twice with MeOH. Yield 43 mg (83%). ^{1}H NMR (400 MHz, DMSO-d_6): δ 0.99 (d, 3H, Me-*i*Pr, *J* = 8 Hz), 1.05 (d, 3H, Me-*i*Pr, *J* = 8 Hz), 2.15 (s, 3H, Me-Ar), 2.64 (m, 1H, CH-Ar), 2.73 (s, Me-*i*Pr), 5.76 (d, 1H, CH (*p*-cym), *J* = 4 Hz), 5.99 (d, 1H, CH (*p*-cym), *J* = 4 Hz), 6.03 (d, 1H, CH (*p*-cym), *J* = 8 Hz), 6.08 (d, 1H, CH (*p*-cym), *J* = 8 Hz), 7.53 (t, 1H, H2-L_1, *J* = 8 Hz), 7.65 (t, 1H, H3-L_1, *J* = 8 Hz), 7.93 (t, 1H, H1-L_1, *J* = 4 Hz), 8.02 (t, 1H, H4-L_1, *J* = 8 Hz), 8.08 (d, 1H, H9-L_1, *J* = 8 Hz), 8.18 (d, 1H, H8-L_1, *J* = 8 Hz), 8.33

https://dx.doi.org/10.1021/acsomega.0c01204
ACS Omega XXXX, XXX, XXX−XXX

(d, 1H, H10-L_1, J = 2 Hz), 8.40 (d, 1H, H7-L_1, J = 8 Hz) ppm. ^{13}C NMR (100 MHz, $CDCl_3$): δ 22.1 (Me-Ar), 22.5 (Me-*i*Pr), 24.1 (Me-*i*Pr), 31.2 (CH-*i*Pr), 80.9 (*p*-cym), 81.3 (*p*-cym), 83.7 (*p*-cym), 84.1 (*p*-cym), 89.5 (*p*-cym), 103.7 (*p*-cym), 123.0 (L_1), 123.4 (L_1), 124.1 (L_1), 126.3 (L_1) 128.0 (L_1), 128.4 (L_1), 128.9 (L_1), 130.3 (L_1), 131.3 (L_1), 132.0 (L_1), 134.4 (L_1), 140.2 (L_1), 141.6 (L_1), 148.0 (L_1), 157.4 (L_1) ppm. IR: 3075 (w), 3059 (w), 3030 (w), 2963 (w), 2867 (w), 1604 (w), 1596 (m), 1497 (s), 1468 (s), 1447 (m), 1420 (m), 1383 (m), 1356 (m), 1327 (m), 1303 (m), 1244 (s), 1212 (m), 1199 (m), 1164 (m), 1140 (m), 1124 (s), 1092 (m), 1068 (m), 1052 (m), 1034 (m), 1012 (m), 970 (m), 946 (m), 871 (s), 794 (s), 765 (s), 749 (s), 725 (s). Found, %: C, 58.40; H, 4.41; N, 8.32. $C_{25}H_{22}N_3OClRu$. Calcd, %: C, 58.08; H, 4.29; N, 8.13.

*[Ru(p-cym) (L_2)Cl] (**2**).* **HL_2** (53 mg, 0.2 mmol) was dissolved in MeOH (1.5 mL). $[Ru(p\text{-cym})Cl_2]_2$ (61.2 mg, 0.1 mmol) was dissolved in MeOH (1.5 mL), and the resulting solution was added to the initial one. After 24 h, red crystals formed were filtered off and washed twice with MeOH. Yield 80 mg (75%). ^{1}H NMR (400 MHz, $CDCl_3$): δ 1.08 (d, 3H, Me-*i*Pr, J = 8 Hz), 1.11 (d, 3H, Me-*i*Pr, J = 8 Hz), 2.16 (s, 3H, Me-Ar), 2.70 (m, 1H, CH-Ar), 5.74 (d, 1H, CH (*p*-cym), J = 8 Hz), 5.925 (d, 1H, CH (*p*-cym), J = 4 Hz), 5.98 (d, 1H, CH (*p*-cym), J = 8 Hz), 6.03 (d, 1H, CH (*p*-cym), J = 8 Hz), 7.45 (t, 1H, H-8, J = 8 Hz), 7.52 (td, 1H, H-9, J = 8 Hz, J = 1.2 Hz), 7.65 (td, 1H, H-2, J = 8 Hz, J = 2.4 Hz), 7.98 (d, 1H, H-4, J = 8 Hz), 8.02 (t, 1H, H-3, J = 4H), 8.03 (dd, 1H, H-7, J = 8 Hz, J = 0.8 Hz), 8.37 (d, 1H, H-1, J = 4 Hz), 8.39 (d, 1H, H-10, J = 4 Hz) ppm. ^{13}C NMR (100 MHz, $CDCl_3$): δ 19.2 (Me-Ar), 22.1 (Me-*i*Pr), 22.6 (Me-*i*Pr), 31.2 (CH-*i*Pr), 83.1 (*p*-cym), 83.4 (*p*-cym), 83.9 (*p*-cym), 88.6 (*p*-cym), 102.5 (*p*-cym), 103.7 (*p*-cym), 116.9 (L_2), 117.7 (L_2), 120.2 (L_2), 121.7 (L_2) 122.9 (L_2), 125.8 (L_2), 127.4 (L_2), 128.1 (L_2), 128.2 (L_2), 128.9 (L_2), 136.2 (L_2), 137.9 (L_2) 146.3 (L_2), 157.0 (L_2), 157.6 (L_2) ppm. IR: 3083 (w), 3062 (w), 3033 (w), 2971 (w), 2873 (w), 1692 (s), 1625 (m), 1593 (m), 1561 (m), 1540 (w), 1495 (s), 1460 (s), 1441 (s), 1404 (m), 1356 (m), 1330 (m), 1316 (m), 1303 (m), 1242 (s), 1191 (m), 1159 (m), 1146 (m), 1124 (m), 1111 (m), 1095 (m), 1055 (m), 1039 (m), 1026 (m), 1007 (m), 940 (m), 868 (m), 807 (s), 794 (m), 759 (s), 743 (s), 727 (m), 709 (m), 687 (s), 674 (m). Found, %: C, 56.58; H, 4.22; N, 7.95. $C_{25}H_{22}N_3O_2ClRu$. Calcd, %: C, 56.34; H, 4.16; N, 7.88.

*[Ru_2(p-cym)$_2$(L_3)Cl_2]·1.5MeOH (**3**).* **HL_3** (24.8 mg, 0.1 mmol) was suspended in MeOH (5 mL) and 1 mL of 0.1 M solution KOH in MeOH was added. Reaction mixture was stirred for 1 h to afford pale yellow precipitate of potassium salt. $[Ru(p\text{-cym})Cl_2]_2$ (30.6 mg, 0.1 mmol) was dissolved in MeOH (2 mL), and solution was added to the initial suspension. The resulting red crystals were filtered, washed with MeOH, and dried at room temperature. Yield 47 mg (55%). ^{1}H NMR (400 MHz, $CDCl_3$): δ 1.08 (dd, 6H, Me-*i*Pr (assymm. *p*-cym), J^1 = 24 Hz, J^2 = 4 Hz), 1.41 (dd, 6H, Me-*i*Pr (symm. *p*-cym), J^1 = 16 Hz, J^2 = 8 Hz), 2.20 (s, 3H, Me-Ar (assymm. *p*-cym)), 2.34 (s, 3H, Me-Ar (symm. *p*-cym)), 2.72 (m, 1H, CH-Ar (assymm. *p*-cym)), 3.10 (m, 1H, CH-Ar (symm. *p*-cym)), 5.30 (d, 1H, CH (symm. *p*-cym), J = 4 Hz), 5.40 (d, 1H, CH (symm. *p*-cym), J = 8 Hz), 5.55 (d, 1H, CH (symm. *p*-cym), J = 4 Hz), 5.58 (d, 1H, CH (symm. *p*-cym), J = 8 Hz), 5.79 (d, 1H, CH (assymm. *p*-cym), J = 8 Hz), 5.96 (d, 1H, CH (assymm. *p*-cym), 8 Hz), 6.02 (d, 1H, CH (assymm. *p*-cym), 4 Hz), 6.19 (d, 1H, CH (assymm. *p*-cym), 8 Hz), 7.51 (t, 1H, H8-L3, J = 8 Hz), 7.67 (t, 1H, H7-L3, J = 8 Hz), 8.10 (d, 1H, H4-L3, J = 4 Hz), 8.23 (t, 2H, H9-L3, J = 8 Hz), 9.23 (d, 1H, H3-L3, J = 8 Hz), 10.10 (s, 1H, H1-L3) ppm. ^{13}C NMR (100 MHz, DMSO-d_6): δ 18.3 (Me-Ar), 18.9 (Me-Ar), 22.9 (Me-*i*Pr), 22.2 (Me-*i*Pr), 22.3 (Me-*i*Pr), 30.4 (CH-*i*Pr) 31.1 (CH-*i*Pr), 83.3 (*p*-cym), 84.1 (*p*-cym), 85.2 (*p*-cym), 85.9 (*p*-cym), 86.8 (*p*-cym), 90.0 (*p*-cym), 100.5 (*p*-cym), 103.3 (*p*-cym), 103.7 (L_3), 106.8 (L_3), 121.9 (L_3), 123.2 (L_3), 124.9 (L_3), 128.3 (L_3), 132.5 (L_3), 134.0 (L_3), 144.4 (L_3), 146.7 (L_3), 146.9 (L_3), 148.8 (L_3), 151.8 (L_3), 157.9 (L_3) ppm. IR: 3051 (w), 2955 (m), 2926 (w), 2873 (w), 1604 (m), 1593 (w), 1561 (w), 1497 (s), 1473 (s), 1412 (s), 1394 (s), 1359 (m), 1316 (s), 1250 (s), 1204 (m), 1154 (s), 1132 (m), 1116 (m), 1068 (m), 1028 (m), 978 (m), 874 (m), 826 (s), 802 (s), 773 (s), 757 (s), 730 (s). Found, %: C, 49.11; H, 4.54; N, 6.43. $C_{35.5}H_{41}Cl_3N_4O_{2.5}Ru_2$. Calcd, %: C, 48.90; H, 4.74; N, 6.42.

*[Ru(p-cym)$_2$(L_4)Cl_2]·0.5DMF (**4**).* **HL_4** (24.8 mg, 0.1 mmol) was suspended in DMF (2.5 mL). $[Ru(p\text{-cym})Cl_2]_2$ (30.6 mg, 0.05 mmol) and was dissolved in MeOH (2.5 mL), and the resulting solution was added to the initial suspension. The mixture was stirred until the ligand was completely dissolved. The resulting red precipitate was filtered, washed with MeOH, and dried at room temperature. Yield 42 mg (81%). ^{1}H NMR (400 MHz, DMSO-d_6): δ 1.005 (d, 3H, Me-*i*Pr, J = 4 Hz), 1.075 (d, 3H, Me-*i*Pr, J = 4 Hz), 2.15 (s, 3H, Me-Ar), 2.68 (m, 1H, CH-Ar), 5.805 (d, 1H, CH (*p*-cym), J = 4 Hz), 6.03 (d, 1H, CH (*p*-cym), J = 8 Hz), 6.045 (d, 1H, CH (*p*-cym), J = 4 Hz), 6.105 (d, 1H, CH (*p*-cym), J = 4 Hz), 7.57 (t, 1H, H8-L_3, J = 8 Hz), 7.70 (t, 1H, H3-L_3, J = 8 Hz), 8.015 (dd, 1H, H9-L_3, J = 12 Hz, J = 4 Hz), 8.09 (d, 1H, H7-L_3, J = 8 Hz), 8.26 (d, 1H, H10-L_3, J = 8 Hz), 8.795 (dd, 1H, H4-L_3, J = 10 Hz, J = 1.6 Hz), 9.195 (dd, 1H, H2-L_3, J = 4 Hz, J = 1.6 Hz) ppm. ^{13}C NMR (100 MHz, $CDCl_3$): δ 21.9 (Me-Ar), 24.1 (Me-*i*Pr), 30.9 (Me-*i*Pr), 31.2 (CH-*i*Pr), 83.6 (*p*-cym), 83.9 (*p*-cym), 85.9 (*p*-cym), 87.0 (*p*-cym), 89.3 (*p*-cym), 100.6 (*p*-cym), 122.8 (L_4), 124.2 (L_4), 124.6 (L_4), 124.6 (L_4) 126.0 (L_4), 126.2 (L_4), 127.3 (L_4), 128.9 (L_4), 132.9 (L_4), 133.9 (L_4), 136.3 (L_4), 138.7 (L_4), 139.7 (L_4), 156.4 (L_4) ppm. IR: 3056 (w), 2971 (w), 2923 (w), 2873 (w), 1679 (s), 1620 (m), 1604 (m), 1569 (m), 1511 (m), 1495 (s), 1476 (s), 1460 (s), 1417 (s), 1380 (m), 1359 (m), 1308 (s), 1282 (m), 1242 (s), 1204 (m), 1175 (m), 1154 (m), 1149 (m), 1111 (m), 1076 (m), 1036 (m), 1007 (m), 996 (m), 959 (m), 911 (m), 890 (m), 876 (m), 820 (m), 797 (m), 775 (s), 762 (s), 738 (m), 690 (m). Found, %: C, 55.03; H, 4.48; N, 11.53. $C_{25.5}H_{24.5}ClN_{4.5}O_{1.5}Ru$. Calcd, %: C, 55.23; H, 4.45; N, 11.37.

■ ASSOCIATED CONTENT

Supporting Information

The Supporting Information is available free of charge at https://pubs.acs.org/doi/10.1021/acsomega.0c01204.

Supplementary crystal structure figures, NCI plots, supplementary computational chemistry figures, UV−Vis spectra, cyclic voltammograms, frontier molecular orbitals data, NMR spectra of the complexes, FT-IR spectra of the complexes, PXRD patterns of the complexes, and NMR spectra of the transfer hydrogenation products (PDF)

Crystallographic data of **1** (CIF)

Crystallographic data of **2** (CIF)

https://dx.doi.org/10.1021/acsomega.0c01204
ACS Omega XXXX, XXX, XXX−XXX

Crystallographic data of **3** (CIF)

Crystallographic data of **4** (CIF)

AUTHOR INFORMATION

Corresponding Authors

Enrico Benassi − *Department of Chemistry, Shihezi University, 832000 Shihezi, Xinjiang, PR China*; Email: enrico.benassi@outlook.com

Andrei S. Potapov − *Nikolaev Institute of Inorganic Chemistry, Siberian Branch of the Russian Academy of Sciences, 630090 Novosibirsk, Russia; Department of Natural Sciences, Novosibirsk State University, 630090 Novosibirsk, Russia*; orcid.org/0000-0003-2360-7473; Email: potapov@niic.nsc.ru

Authors

Vladislava V. Matveevskaya − *Kizhner Research Center, National Research Tomsk Polytechnic University, 634050 Tomsk, Russia*

Dmitry I. Pavlov − *Kizhner Research Center, National Research Tomsk Polytechnic University, 634050 Tomsk, Russia*

Taisiya S. Sukhikh − *Nikolaev Institute of Inorganic Chemistry, Siberian Branch of the Russian Academy of Sciences, 630090 Novosibirsk, Russia; Department of Natural Sciences, Novosibirsk State University, 630090 Novosibirsk, Russia*; orcid.org/0000-0001-5269-9130

Artem L. Gushchin − *Nikolaev Institute of Inorganic Chemistry, Siberian Branch of the Russian Academy of Sciences, 630090 Novosibirsk, Russia; Department of Natural Sciences, Novosibirsk State University, 630090 Novosibirsk, Russia*

Alexander Yu. Ivanov − *Center for Magnetic Resonance, Saint Petersburg State University, 198504 Peterhof, Russia*

Tatiana B. Tennikova − *Institute of Chemistry, Saint Petersburg State University, 198504 Peterhof, Russia*

Vladimir V. Sharoyko − *Institute of Chemistry, Saint Petersburg State University, 198504 Peterhof, Russia*

Sergey V. Baykov − *Institute of Chemistry, Saint Petersburg State University, 198504 Peterhof, Russia*; orcid.org/0000-0002-8912-5816

Complete contact information is available at: https://pubs.acs.org/10.1021/acsomega.0c01204

Author Contributions

The manuscript was written through contributions of all authors.

Funding

The reported study was funded by RFBR according to the research project no. 18-33-00676.

Notes

The authors declare no competing financial interest.

ACKNOWLEDGMENTS

NMR studies of the complexes were performed at the Research Centre for Magnetic Resonance of Saint Petersburg State University Research Park. The Siberian Branch of the Russian Academy of Sciences (SB RAS) Siberian Supercomputer Center is gratefully acknowledged for providing supercomputer facilities. The authors thank Dr. Irina Mirzaeva for recording the NMR spectra.

REFERENCES

(1) Al-Masoudi, W. A.; Al-Masoudi, N. A.; Weibert, B.; Winter, R. Synthesis, X-Ray Structure, in Vitro HIV and Kinesin Eg5 Inhibition Activities of New Arene Ruthenium Complexes of Pyrimidine Analogs. *J. Coord. Chem.* **2017**, *70*, 2061−2073.

(2) Carcelli, M.; Bacchi, A.; Pelagatti, P.; Rispoli, G.; Rogolino, D.; Sanchez, T. W.; Sechi, M.; Neamati, N. Ruthenium Arene Complexes as HIV-1 Integrase Strand Transfer Inhibitors. *J. Inorg. Biochem.* **2013**, *118*, 74−82.

(3) Allardyce, C. S.; Dyson, P. J.; Ellis, D. J.; Salter, P. A.; Scopelliti, R. Synthesis and Characterisation of Some Water Soluble Ruthenium(II)-Arene Complexes and an Investigation of Their Antibiotic and Antiviral Properties. *J. Organomet. Chem.* **2003**, *668*, 35−42.

(4) Li, S.; Wu, C.; Tang, X.; Gao, S.; Zhao, X.; Yan, H.; Wang, X. New Strategy for Reversing Biofilm-Associated Antibiotic Resistance through Ferrocene-Substituted Carborane Ruthenium(II)-Arene Complex. *Sci. China: Chem.* **2013**, *56*, 595−603.

(5) Kong, Y.; Chen, F.; Su, Z.; Qian, Y.; Wang, F.-x.; Wang, X.; Zhao, J.; Mao, Z.-W.; Liu, H.-K. Bioactive Ruthenium(II)-Arene Complexes Containing Modified 18β-Glycyrrhetinic Acid Ligands. *J. Inorg. Biochem.* **2018**, *182*, 194−199.

(6) Ude, Z.; Romero-Canelón, I.; Twamley, B.; Fitzgerald Hughes, D.; Sadler, P. J.; Marmion, C. J. A Novel Dual-Functioning Ruthenium(II)−Arene Complex of an Anti-Microbial Ciprofloxacin Derivative — Anti-Proliferative and Anti-Microbial Activity. *J. Inorg. Biochem.* **2016**, *160*, 210−217.

(7) Murray, B. S.; Babak, M. V.; Hartinger, C. G.; Dyson, P. J. The Development of RAPTA Compounds for the Treatment of Tumors. *Coordination Chemistry Reviews*; Elsevier, January 1, 2016, pp 86−114.

(8) Nazarov, A. A.; Hartinger, C. G.; Dyson, P. J. Opening the Lid on Piano-Stool Complexes: An Account of Ruthenium(II)−Arene Complexes with Medicinal Applications. *J. Organomet. Chem.* **2014**, *751*, 251−260.

(9) Pettinari, R.; Marchetti, F.; Di Nicola, C.; Pettinari, C. Half-Sandwich Metal Complexes with β-Diketone-Like Ligands and Their Anticancer Activity. *Eur. J. Inorg. Chem.* **2018**, *2018*, 3521−3536.

(10) Zhang, P.; Sadler, P. J. Advances in the Design of Organometallic Anticancer Complexes. *J. Organomet. Chem.* **2017**, *839*, 5−14.

(11) Allardyce, C. S.; Dyson, P. J.; Ellis, D. J.; Heath, S. L. [Ru(H6-p-Cymene)Cl2(Pta)] (Pta = 1,3,5-Triaza-7-Phosphatricyclo[3.3.1.1]-Decane): A Water Soluble Compound That Exhibits PH Dependent DNA Binding Providing Selectivity for Diseased Cells. *Chem. Commun.* **2001**, *15*, 1396−1397.

(12) Weiss, A.; Berndsen, R. H.; Dubois, M.; Müller, C.; Schibli, R.; Griffioen, A. W.; Dyson, P. J.; Nowak-Sliwinska, P. In *Vivo* Anti-Tumor Activity of the Organometallic Ruthenium(Ii)-Arene Complex [Ru(η^6 - p -Cymene)Cl_2 (Pta)] (RAPTA-C) in Human Ovarian and Colorectal Carcinomas. *Chem. Sci.* **2014**, *5*, 4742−4748.

(13) Koepf-Maier, P.; Koepf, H. Non-Platinum Group Metal Antitumor Agents. History, Current Status, and Perspectives. *Chem. Rev.* **1987**, *87*, 1137−1152.

(14) Guichard, S. M.; Else, R.; Reid, E.; Zeitlin, B.; Aird, R.; Muir, M.; Dodds, M.; Fiebig, H.; Sadler, P. J.; Jodrell, D. I. Anti-Tumour Activity in Non-Small Cell Lung Cancer Models and Toxicity Profiles for Novel Ruthenium(II) Based Organo-Metallic Compounds. *Biochem. Pharmacol.* **2006**, *71*, 408−415.

(15) Aird, R. E.; Cummings, J.; Ritchie, A. A.; Muir, M.; Morris, R. E.; Chen, H.; Sadler, P. J.; Jodrell, D. I. In Vitro and in Vivo Activity and Cross Resistance Profiles of Novel Ruthenium (II) Organometallic Arene Complexes in Human Ovarian Cancer. *Br. J. Cancer* **2002**, *86*, 1652−1657.

(16) Morris, R. E.; Aird, R. E.; Del Socorro Murdoch, P.; Chen, H.; Cummings, J.; Hughes, N. D.; Parsons, S.; Parkin, A.; Boyd, G.; Jodrell, D. I.; Sadler, P. J. Inhibition of Cancer Cell Growth by Ruthenium(II) Arene Complexes. *J. Med. Chem.* **2001**, *44*, 3616−3621.

(17) Marchetti, F.; Pettinari, R.; Di Nicola, C.; Pettinari, C.; Palmucci, J.; Scopelliti, R.; Riedel, T.; Therrien, B.; Galindo, A.; Dyson, P. J. Synthesis, Characterization and Cytotoxicity of Arene−Ruthenium(Ii) Complexes with Acylpyrazolones Functionalized with Aromatic Groups in the Acyl Moiety. *Dalton Trans.* **2018**, *47*, 868−878.
(18) Ohkuma, T.; Utsumi, N.; Tsutsumi, K.; Murata, K.; Sandoval, C.; Noyori, R. The Hydrogenation/Transfer Hydrogenation Network: Asymmetric Hydrogenation of Ketones with Chiral H6 -Arene/ N -Tosylethylenediamine−Ruthenium(II) Catalysts. *J. Am. Chem. Soc.* **2006**, *128*, 8724−8725.
(19) Štěpnička, P.; Ludvík, J.; Canivet, J.; Süss-Fink, G. Relating Catalytic Activity and Electrochemical Properties: The Case of Arene−Ruthenium Phenanthroline Complexes Catalytically Active in Transfer Hydrogenation. *Inorg. Chim. Acta* **2006**, *359*, 2369−2374.
(20) Kumar, S.; Gupta, S. K. The First Examples of Discotic Liquid Crystalline Gemini Surfactants. *Tetrahedron Lett.* **2010**, *51*, 5459−5462.
(21) Soriano, M. L.; Jalón, F. A.; Manzano, B. R.; Maestro, M. Synthesis and Characterization of Ru(Arene) Complexes of Bispyrazolylazines: Catalytic Hydrogen Transfer of Ketones. *Inorg. Chim. Acta* **2009**, *362*, 4486−4492.
(22) Biancalana, L.; Abdalghani, I.; Chiellini, F.; Zacchini, S.; Pampaloni, G.; Crucianelli, M.; Marchetti, F. Ruthenium Arene Complexes with α-Aminoacidato Ligands: New Insights into Transfer Hydrogenation Reactions and Cytotoxic Behaviour. *Eur. J. Inorg. Chem.* **2018**, *2018*, 3041−3057.
(23) Rautenstrauch, V.; Hoang-Cong, X.; Churlaud, R.; Abdur-Rashid, K.; Morris, R. H. Hydrogenation versus Transfer Hydrogenation of Ketones: Two Established Ruthenium Systems Catalyze Both. *Chem.—Eur. J.* **2003**, *9*, 4954−4967.
(24) Blaser, H.-U.; Malan, C.; Pugin, B.; Spindler, F.; Steiner, H.; Studer, M. Selective Hydrogenation for Fine Chemicals: Recent Trends and New Developments. *Adv. Synth. Catal.* **2003**, *345*, 103−151.
(25) Clapham, S. E.; Hadzovic, A.; Morris, R. H. Mechanisms of the H2-Hydrogenation and Transfer Hydrogenation of Polar Bonds Catalyzed by Ruthenium Hydride Complexes. *Coord. Chem. Rev.* **2004**, *248*, 2201−2237.
(26) Shi, J.; Hu, B.; Chen, X.; Shang, S.; Deng, D.; Sun, Y.; Shi, W.; Yang, X.; Chen, D. Synthesis, Reactivity, and Catalytic Transfer Hydrogenation Activity of Ruthenium Complexes Bearing NNN Tridentate Ligands: Influence of the Secondary Coordination Sphere. *ACS Omega* **2017**, *2*, 3406−3416.
(27) Xu, S.; Kalapugama, S.; Rasu, L.; Bergens, S. H. Preparation and Study of Reusable Polymerized Catalysts for Ester Hydrogenation. *ACS Omega* **2019**, *4*, 12212−12221.
(28) Castarlenas, R.; Sémeril, D.; Noels, A. F.; Demonceau, A.; Dixneuf, P. H. Allenylidene-Ruthenium-Arene Precatalyst for Ring Opening Metathesis Polymerisation (ROMP). *J. Organomet. Chem.* **2002**, *663*, 235−238.
(29) Castarlenas, R.; Dixneuf, P. H. Highly Active Catalysts in Alkene Metathesis: First Observed Transformation of Allenylidene into Indenylidene via Alkenylcarbyne—Ruthenium Species. *Angew. Chem., Int. Ed.* **2003**, *42*, 4524−4527.
(30) Castarlenas, R.; Vovard, C.; Fischmeister, C.; Dixneuf, P. H. Allenylidene-to-Indenylidene Rearrangement in Arene−Ruthenium Complexes: A Key Step to Highly Active Catalysts for Olefin Metathesis Reactions. *J. Am. Chem. Soc.* **2006**, *128*, 4079−4089.
(31) Schepetkin, I. A.; Khlebnikov, A. I.; Potapov, A. S.; Kovrizhina, A. R.; Matveevskaya, V. V.; Belyanin, M. L.; Atochin, D. N.; Zanoza, S. O.; Gaidarzhy, N. M.; Lyakhov, S. A.; Kirpotina, L. N.; Quinn, M. T. Synthesis, Biological Evaluation, and Molecular Modeling of 11H-Indeno[1,2-b]Quinoxalin-11-One Derivatives and Tryptanthrin-6-Oxime as c-Jun N-Terminal Kinase Inhibitors. *Eur. J. Med. Chem.* **2019**, *161*, 179−191.
(32) Schepetkin, I. A.; Kirpotina, L. N.; Khlebnikov, A. I.; Hanks, T. S.; Kochetkova, I.; Pascual, D. W.; Jutila, M. A.; Quinn, M. T. Identification and Characterization of a Novel Class of C-Jun N-Terminal Kinase Inhibitors. *Mol. Pharmacol.* **2012**, *81*, 832−845.
(33) Schepetkin, I. A.; Kirpotina, L. N.; Hammaker, D.; Kochetkova, I.; Khlebnikov, A. I.; Lyakhov, S. A.; Firestein, G. S.; Quinn, M. T. Anti-Inflammatory Effects and Joint Protection in Collagen-Induced Arthritis after Treatment with IQ-1S, a Selective c-Jun N-Terminal Kinase Inhibitor. *J. Pharmacol. Exp. Ther.* **2015**, *353*, 505−516.
(34) Stankevich, K. S.; Schepetkin, I. A.; Goreninskii, S. I.; Lavrinenko, A. K.; Bolbasov, E. N.; Kovrizhina, A. R.; Kirpotina, L. N.; Filimonov, V. D.; Khlebnikov, A. I.; Tverdokhlebov, S. I.; Quinn, M. T. Poly(ε-Caprolactone) Scaffolds Doped with c-Jun N-Terminal Kinase Inhibitors Modulate Phagocyte Activation. *ACS Biomater. Sci. Eng.* **2019**, *5*, 5990−5999.
(35) Kibler, E.; Lavrinenko, A.; Kolesnik, I.; Stankevich, K.; Bolbasov, E.; Kudryavtseva, V.; Leonov, A.; Schepetkin, I.; Khlebnikov, A.; Quinn, M. T.; Tverdokhlebov, S. Electrosprayed Poly(Lactic-Co-Glycolic Acid) Particles as a Promising Drug Delivery System for the Novel JNK Inhibitor IQ-1. *Eur. Polym. J.* **2020**, *127*, 109598.
(36) Atochin, D. N.; Schepetkin, I. A.; Khlebnikov, A. I.; Seledtsov, V. I.; Swanson, H.; Quinn, M. T.; Huang, P. L. A Novel Dual NO-Donating Oxime and c-Jun N-Terminal Kinase Inhibitor Protects against Cerebral Ischemia−Reperfusion Injury in Mice. *Neurosci. Lett.* **2016**, *618*, 45−49.
(37) Plotnikov, M. B.; Chernysheva, G. A.; Aliev, O. I.; Smol'iakova, V. I.; Fomina, T. I.; Osipenko, A. N.; Rydchenko, V. S.; Anfinogenova, Y. J.; Khlebnikov, A. I.; Schepetkin, I. A.; Atochin, D. N. Protective Effects of a New C-Jun N-Terminal Kinase Inhibitor in the Model of Global Cerebral Ischemia in Rats. *Molecules* **2019**, *24*, 1722.
(38) Zhang, C.; Li, S.; Ji, L.; Liu, S.; Li, Z.; Li, S.; Meng, X. Design, Synthesis and Antitumor Activity of Non-Camptothecin Topoisomerase I Inhibitors. *Bioorg. Med. Chem. Lett.* **2015**, *25*, 4693−4696.
(39) Tseng, C.-H.; Chen, Y.-R.; Tzeng, C.-C.; Liu, W.; Chou, C.-K.; Chiu, C.-C.; Chen, Y.-L. Discovery of Indeno[1,2-b]Quinoxaline Derivatives as Potential Anticancer Agents. *Eur. J. Med. Chem.* **2016**, *108*, 258−273.
(40) Wu, X.; Li, X.; Li, Z.; Yu, Y.; You, Q.; Zhang, X. Discovery of Nonquinone Substrates for NAD(P)H: Quinone Oxidoreductase 1 (NQO1) as Effective Intracellular ROS Generators for the Treatment of Drug-Resistant Non-Small-Cell Lung Cancer. *J. Med. Chem.* **2018**, *61*, 11280−11297.
(41) Kaur, R.; Manjal, S. K.; Rawal, R. K.; Kumar, K. Recent Synthetic and Medicinal Perspectives of Tryptanthrin. *Bioorg. Med. Chem.* **2017**, *25*, 4533−4552.
(42) Jung, E. H.; Jung, J. Y.; Ko, H. L.; Kim, J. K.; Park, S. M.; Jung, D. H.; Park, C. A.; Kim, Y. W.; Ku, S. K.; Cho, I. J.; Kim, S. C. Tryptanthrin Prevents Oxidative Stress-Mediated Apoptosis through AMP-Activated Protein Kinase-Dependent P38 Mitogen-Activated Protein Kinase Activation. *Arch. Pharmacal Res.* **2017**, *40*, 1071−1086.
(43) Krivogorsky, B.; Grundt, P.; Yolken, R.; Jones-Brando, L. Inhibition of Toxoplasma Gondii</Em> by Indirubin and Tryptanthrin Analogs. *Antimicrob. Agents Chemother.* **2008**, *52*, 4466−4469.
(44) Hwang, J.-M.; Oh, T.; Kaneko, T.; Upton, A. M.; Franzblau, S. G.; Ma, Z.; Cho, S.-N.; Kim, P. Design, Synthesis, and Structure−Activity Relationship Studies of Tryptanthrins As Antitubercular Agents. *J. Nat. Prod.* **2013**, *76*, 354−367.
(45) Tsai, Y.-C.; Lee, C.-L.; Yen, H.-R.; Chang, Y.-S.; Lin, Y.-P.; Huang, S.-H.; Lin, C.-W. Antiviral Action of Tryptanthrin Isolated from Strobilanthes Cusia Leaf against Human Coronavirus NL63. *Biomolecules* . **2020**, *10*. DOI: 10.3390/biom10030366.
(46) Shankar G, M.; Alex, V. V.; Nisthul A, A.; Bava, S.; Sundaram, S.; Retnakumari, A. P.; Chittalakkottu, S.; Anto, R. J. Pre-clinical evidences for the efficacy of tryptanthrin as a potent suppressor of skin cancer. *Cell Proliferation* **2020**, *53*, No. e12710.

https://dx.doi.org/10.1021/acsomega.0c01204
ACS Omega XXXX, XXX, XXX−XXX

(47) Mexia, N.; Koutrakis, S.; He, G.; Skaltsounis, A.-L.; Denison, M. S.; Magiatis, P. A Biomimetic, One-Step Transformation of Simple Indolic Compounds to Malassezia-Related Alkaloids with High AhR Potency and Efficacy. *Chem. Res. Toxicol.* **2019**, *32*, 2238−2249.
(48) Wang, Q.; Liang, J.; Brennan, C.; Ma, L.; Li, Y.; Lin, X.; Liu, H.; Wu, J. Anti-inflammatory effect of alkaloids extracted from Dendrobium aphyllum on macrophage RAW 264.7 cells through NO production and reduced IL-1, IL-6, TNF-α and PGE2 expression. *Int. J. Food Sci. Technol.* **2020**, *55*, 1255−1264.
(49) Canaj, A. B.; Nodaraki, L. E.; Ślepokura, K.; Siczek, M.; Tzimopoulos, D. I.; Lis, T.; Milios, C. J. A Family of Polynuclear Cobalt Complexes upon Employment of an Indeno-Quinoxaline Based Oxime Ligand. *RSC Adv.* **2014**, *4*, 23068−23077.
(50) Canaj, A. B.; Nodaraki, L. E.; Philippidis, A.; Tzimopoulos, D. I.; Fotopoulou, E.; Siczek, M.; Lis, T.; Milios, C. J. An Indeno-Quinoxaline Based Oxime Ligand for the Synthesis of Polynuclear Ni(Ii) Clusters. *RSC Adv.* **2013**, *3*, 13214.
(51) Adhikari, S.; Palepu, N. R.; Sutradhar, D.; Shepherd, S. L.; Phillips, R. M.; Kaminsky, W.; Chandra, A. K.; Kollipara, M. R. Neutral and Cationic Half-Sandwich Arene Ruthenium, Cp*Rh and Cp*Ir Oximato and Oxime Complexes: Synthesis, Structural, DFT and Biological Studies. *J. Organomet. Chem.* **2016**, *820*, 70−81.
(52) Palepu, N. R.; Adhikari, S.; J, R. P.; Verma, A. K.; Shepherd, S. L.; Phillips, R. M.; Kaminsky, W.; Kollipara, M. R. Half-Sandwich Ruthenium, Rhodium and Iridium Complexes Featuring Oxime Ligands: Structural Studies and Preliminary Investigation of *in Vitro* and *in Vivo* Anti-Tumour Activities. *Appl. Organomet. Chem.* **2017**, *31*, No. e3640.
(53) de la Cueva-Alique, I.; Sierra, S.; Muñoz-Moreno, L.; Pérez-Redondo, A.; Bajo, A. M.; Marzo, I.; Gude, L.; Cuenca, T.; Royo, E. Biological Evaluation of Water Soluble Arene Ru(II) Enantiomers with Amino-Oxime Ligands. *J. Inorg. Biochem.* **2018**, *183*, 32−42.
(54) Adhikari, S.; Kaminsky, W.; Rao, K. M. Study of the Bonding Modes of Di-2-Pyridyl Ketoxime Ligand towards Ruthenium, Rhodium and Iridium Half Sandwich Complexes. *Z. Anorg. Allg. Chem.* **2016**, *642*, 941−946.
(55) Fernández, R.; Melchart, M.; Habtemariam, A.; Parsons, S.; Sadler, P. J. Use of Chelating Ligands to Tune the Reactive Site of Half-Sandwich Ruthenium(II)−Arene Anticancer Complexes. *Chem.—Eur. J.* **2004**, *10*, 5173−5179.
(56) Peacock, A. F. A.; Melchart, M.; Deeth, R. J.; Habtemariam, A.; Parsons, S.; Sadler, P. J. Osmium(II) and Ruthenium(II) Arene Maltolato Complexes: Rapid Hydrolysis and Nucleobase Binding. *Chem.—Eur. J.* **2007**, *13*, 2601−2613.
(57) Bernet, L.; Lalrempuia, R.; Ghattas, W.; Mueller-Bunz, H.; Vigara, L.; Llobet, A.; Albrecht, M. Tunable Single-Site Ruthenium Catalysts for Efficient Water Oxidation. *Chem. Commun.* **2011**, *47*, 8058.
(58) Rüther, T.; Woodward, C. P.; Jones, T. W.; Coghlan, C. J.; Hebting, Y.; Cordiner, R. L.; Dawson, R. E.; Robinson, D. E. J. E.; Wilson, G. J. Synthesis, Characterisation, and Properties of p-Cymene Ruthenium(II) Tetracarboxylate Bipyridine Complexes [(H6-p-Cymene)Ru(Rn,Rn′-Tcbpy)Cl][Cl]. *J. Organomet. Chem.* **2016**, *823*, 136−146.
(59) Daunys, S.; Matulis, D.; Petrikaitė, V. Synergistic Activity of Hsp90 Inhibitors and Anticancer Agents in Pancreatic Cancer Cell Cultures. *Sci. Rep.* **2019**, *9*, 16177.
(60) Kurata, N.; Fujita, H.; Ohuchida, K.; Mizumoto, K.; Mahawithitwong, P.; Sakai, H.; Onimaru, M.; Manabe, T.; Ohtsuka, T.; Tanaka, M. Predicting the Chemosensitivity of Pancreatic Cancer Cells by Quantifying the Expression Levels of Genes Associated with the Metabolism of Gemcitabine and 5-Fluorouracil. *Int. J. Oncol.* **2011**, *39*, 473−482.
(61) APEX2 (Version 2.0), SAINT (Version 8.18c), and SADABS (Version 2.11), Bruker Advanced X-Ray Solutions, Bruker AXS Inc., Madison, Wisconsin, USA, 2000−2012.
(62) Sheldrick, G. M. SHELXT - Integrated Space-Group and Crystal-Structure Determination. *Acta Crystallogr., Sect. A: Found. Crystallogr.* **2015**, *71*, 3−8.
(63) Sheldrick, G. M.; IUCr. Crystal Structure Refinement with *SHELXL*. *Acta Crystallogr., Sect. C: Struct. Chem.* **2015**, *71*, 3−8.
(64) Dolomanov, O. V.; Bourhis, L. J.; Gildea, R. J.; Howard, J. A. K.; Puschmann, H. *OLEX2*: A Complete Structure Solution, Refinement and Analysis Program. *J. Appl. Crystallogr.* **2009**, *42*, 339−341.
(65) Hubina, A. V.; Pogodaev, A. A.; Sharoyko, V. V.; Vlakh, E. G.; Tennikova, T. B. Self-Assembled Spin-Labeled Nanoparticles Based on Poly(Amino Acids). *React. Funct. Polym.* **2016**, *100*, 173−180.
(66) Frisch, M. J.; Trucks, G. W.; Schlegel, H. B.; Scuseria, G. E.; Robb, M. A.; Cheeseman, J. R.; Scalmani, G.; Barone, V.; Mennucci, B.; Petersson, G. A.; Nakatsuji, H.; Caricato, M.; Li, X.; Hratchian, H. P.; Izmaylov, A. F.; Bloino, J.; Zheng, G.; Sonnenberg, J. L.; Hada, M.; Ehara, M.; Toyota, K.; Fukuda, R.; Hasegawa, J.; Ishida, M.; Nakajima, T.; Honda, Y.; Kitao, O.; Nakai, H.; Vreven, T.; Montgomery, J. A.; Peralta, J. E.; Ogliaro, F.; Bearpark, M.; Heyd, J. J.; Brothers, E.; Kudin, K. N.; Staroverov, V. N.; Kobayashi, R.; Normand, J.; Raghavachari, K.; Rendell, A.; Burant, J. C.; Iyengar, S. S.; Tomasi, J.; Cossi, M.; Rega, N.; Millam, J. M.; Klene, M.; Knox, J. E.; Cross, J. B.; Bakken, V.; Adamo, C.; Jaramillo, J.; Gomperts, R.; Stratmann, R. E.; Yazyev, O.; Austin, A. J.; Cammi, R.; Pomelli, C.; Ochterski, J. W.; Martin, R. L.; Morokuma, K.; Zakrzewski, V. G.; Voth, G. A.; Salvador, P.; Dannenberg, J. J.; Dapprich, S.; Daniels, A. D.; Farkas; Foresman, J. B.; Ortiz, J. V.; Cioslowski, J.; Fox, D. J. *Gaussian 09, Revision D.01.* ; Gaussian, Inc.: Wallingford CT, 2013.
(67) Becke, A. D. Density-Functional Exchange-Energy Approximation with Correct Asymptotic Behavior. *Phys. Rev. A: At., Mol., Opt. Phys.* **1988**, *38*, 3098−3100.
(68) Lee, C.; Yang, W.; Parr, R. G. Development of the Colle-Salvetti Correlation-Energy Formula into a Functional of the Electron Density. *Phys. Rev. B: Condens. Matter Mater. Phys.* **1988**, *37*, 785−789.
(69) Vosko, S. H.; Wilk, L.; Nusair, M. Accurate Spin-Dependent Electron Liquid Correlation Energies for Local Spin Density Calculations: A Critical Analysis. *Can. J. Phys.* **1980**, *58*, 1200−1211.
(70) Stephens, P. J.; Devlin, F. J.; Chabalowski, C. F.; Frisch, M. J. Ab Initio Calculation of Vibrational Absorption and Circular Dichroism Spectra Using Density Functional Force Fields. *J. Phys. Chem.* **1994**, *98*, 11623−11627.
(71) McLean, A. D.; Chandler, G. S. Contracted Gaussian Basis Sets for Molecular Calculations. I. Second Row Atoms, *Z* =11−18. *J. Chem. Phys.* **1980**, *72*, 5639−5648.
(72) Krishnan, R.; Binkley, J. S.; Seeger, R.; Pople, J. A. Self-consistent Molecular Orbital Methods. XX. A Basis Set for Correlated Wave Functions. *J. Chem. Phys.* **1980**, *72*, 650−654.
(73) Clark, T.; Chandrasekhar, J.; Spitznagel, G. n. W.; Schleyer, P. V. R. Efficient Diffuse Function-augmented Basis Sets for Anion Calculations. III. The 3-21+G Basis Set for First-row Elements, Li−F. *J. Comput. Chem.* **1983**, *4*, 294−301.
(74) Frisch, M. J.; Pople, J. A.; Binkley, J. S. Self-consistent Molecular Orbital Methods 25. Supplementary Functions for Gaussian Basis Sets. *J. Chem. Phys.* **1984**, *80*, 3265−3269.
(75) Hay, P. J.; Wadt, W. R. *Ab Initio* Effective Core Potentials for Molecular Calculations. Potentials for K to Au Including the Outermost Core Orbitals. *J. Chem. Phys.* **1985**, *82*, 299−310.
(76) Hay, P. J.; Wadt, W. R. *Ab Initio* Effective Core Potentials for Molecular Calculations. Potentials for the Transition Metal Atoms Sc to Hg. *J. Chem. Phys.* **1985**, *82*, 270−283.
(77) Tomasi, J.; Mennucci, B.; Cancès, E. The IEF Version of the PCM Solvation Method: An Overview of a New Method Addressed to Study Molecular Solutes at the QM Ab Initio Level. *J. Mol. Struct.: THEOCHEM* **1999**, *464*, 211−226.
(78) Hirata, S.; Head-Gordon, M. Time-Dependent Density Functional Theory within the Tamm−Dancoff Approximation. *Chem. Phys. Lett.* **1999**, *314*, 291−299.

https://dx.doi.org/10.1021/acsomega.0c01204
ACS Omega XXXX, XXX, XXX−XXX

(79) Yanai, T.; Tew, D. P.; Handy, N. C. A New Hybrid Exchange−Correlation Functional Using the Coulomb-Attenuating Method (CAM-B3LYP). *Chem. Phys. Lett.* **2004**, *393*, 51−57.
(80) Chai, J.-D.; Head-Gordon, M. Long-Range Corrected Hybrid Density Functionals with Damped Atom−Atom Dispersion Corrections. *Phys. Chem. Chem. Phys.* **2008**, *10*, 6615.
(81) Martin, R. L. Natural Transition Orbitals. *J. Chem. Phys.* **2003**, *118*, 4775−4777.
(82) Zhao, Y.; Truhlar, D. G. The M06 Suite of Density Functionals for Main Group Thermochemistry, Thermochemical Kinetics, Noncovalent Interactions, Excited States, and Transition Elements: Two New Functionals and Systematic Testing of Four M06-Class Functionals and 12 Other Function. *Theor. Chem. Acc.* **2008**, *120*, 215−241.
(83) Marenich, A. V.; Cramer, C. J.; Truhlar, D. G. Universal Solvation Model Based on Solute Electron Density and on a Continuum Model of the Solvent Defined by the Bulk Dielectric Constant and Atomic Surface Tensions. *J. Phys. Chem. B* **2009**, *113*, 6378−6396.
(84) Bohórquez, H. J.; Matta, C. F.; Boyd, R. J. The Localized Electrons Detector as an Ab Initio Representation of Molecular Structures. *Int. J. Quantum Chem.* **2010**, *110*, a−n.
(85) Johnson, E. R.; Keinan, S.; Mori-Sánchez, P.; Contreras-García, J.; Cohen, A. J.; Yang, W. Revealing Noncovalent Interactions. *J. Am. Chem. Soc.* **2010**, *132*, 6498−6506.
(86) Boto, R. A.; Contreras-García, J.; Tierny, J.; Piquemal, J.-P. Interpretation of the Reduced Density Gradient. *Mol. Phys.* **2016**, *114*, 1406−1414.
(87) Andrés, J.; Berski, S.; Contreras-García, J.; González-Navarrete, P. Following the Molecular Mechanism for the NH3 + LiH → LiNH2 + H2 Chemical Reaction: A Study Based on the Joint Use of the Quantum Theory of Atoms in Molecules (QTAIM) and Noncovalent Interaction (NCI) Index. *J. Phys. Chem. A* **2014**, *118*, 1663−1672.
(88) Zhang, Y.; He, H.; Dong, K.; Fan, M.; Zhang, S. A DFT Study on Lignin Dissolution in Imidazolium-Based Ionic Liquids. *RSC Adv.* **2017**, *7*, 12670−12681.

https://dx.doi.org/10.1021/acsomega.0c01204
ACS Omega XXXX, XXX, XXX−XXX